NMR Spectroscopy

DOI: 10.1002/anie.201400178

Next-Generation Heteronuclear Decoupling for High-Field Biomolecular NMR Spectroscopy**

Franz Schilling, Lisa R. Warner, Naum I. Gershenzon, Thomas E. Skinner, Michael Sattler,* and Steffen J. Glaser**

Abstract: *Ultra-high-field NMR spectroscopy requires an increased bandwidth for heteronuclear decoupling, especially in biomolecular NMR applications. Composite pulse decoupling cannot provide sufficient bandwidth at practical power levels, and adiabatic pulse decoupling with sufficient bandwidth is compromised by sideband artifacts. A novel low-power, broadband heteronuclear decoupling pulse is presented that generates minimal, ultra-low sidebands. The pulse was derived using optimal control theory and represents a new generation of decoupling pulses free from the constraints of periodic and cyclic sequences. In comparison to currently available state-of-the-art methods this novel pulse provides greatly improved decoupling performance that satisfies the demands of high-field biomolecular NMR spectroscopy.*

High-field magnets are essential for greatly increasing the sensitivity and resolution in NMR studies of biomacromolecules. However, higher magnetic fields also require increased bandwidth to decouple multiplet splittings of peaks, constrained by the power limits of modern cryogenically cooled probes (cryoprobes) and sample heating. This is particularly critical for ^{13}C decoupling, where the ^{13}C chemical shifts found in proteins and nucleic acids span a bandwidth as large as 45 kHz at magnetic fields corresponding to 1.2 GHz proton Larmor frequency (Figure 1).

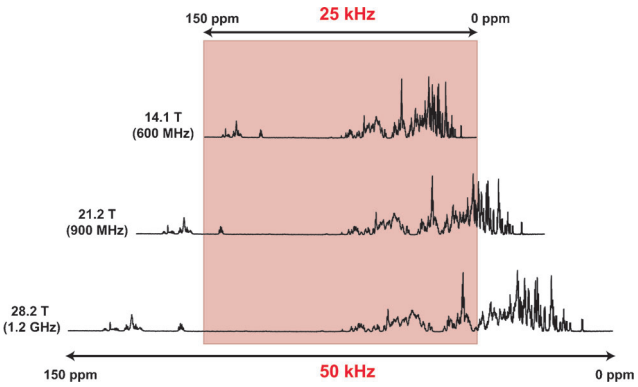

Figure 1. Schematic representation of the maximum decoupling bandwidth of GARP-4 (25 kHz, in red, at recommended cryoprobe $\gamma B_{1,RMS}/(2\pi) = 4.5$ kHz) overlaid on a ^{13}C carbon spectrum of ^{13}C uniformly labeled ubiquitin at 600 MHz and scaled to represent a frequency spread of 37.5 kHz at 900 MHz and 50 kHz at 1.2 GHz.

The first heteronuclear decoupling was accomplished with low-bandwidth continuous-wave irradiation[1] and noise decoupling.[2] Broadband sequences were then developed based on the principle of combining the best broadband inversion pulse[3] with specific phase cycles and supercycles,[3,4] or multiple rotating frame techniques.[5] Composite inversion pulses provide reasonable bandwidth performance for a given pulse power level and are adequate for broadband decoupling defined by the high-field magnets of a previous era. Even larger bandwidths can be achieved at the same power using shaped adiabatic pulses, which provide sufficient bandwidth for ^{13}C decoupling at currently existing magnetic fields.

However, both composite pulse and adiabatic decoupling sequences suffer from intrinsic sideband artifacts, which complicate the analysis of decoupled spectra in biomolecular NMR applications. Thus, sideband artifacts, which stem from the periodic cycling of the decoupling sequence and incomplete refocusing of the coupling evolution, are a significant problem in practical applications. For experiments such as NOESY, where the cross-peak intensity is a few percent of the diagonal peak, sideband artifacts as small as 0.5% of the

[*] Dr. F. Schilling,[+] Prof. Dr. S. J. Glaser
Department Chemie, Technische Universität München
Lichtenbergstr. 4, 85747 Garching (Germany)
E-mail: glaser@tum.de
Homepage: http://www.org.chemie.tu-muenchen.de/glaser
Dr. L. R. Warner,[+] Prof. Dr. M. Sattler
Institute of Structural Biology, Helmholtz Zentrum München
Ingolstädter Landstr. 1, 85764 Neuherberg (Germany)
and
Center for Integrated Protein Science Munich at Biomolecular NMR, Technische Universität München
Lichtenbergstr. 4, 85747 Garching (Germany)
E-mail: sattler@helmholtz-muenchen.de
Homepage: http://www.helmholtz-muenchen.de/en/stb
http://www.nmr.ch.tum.de
Dr. N. I. Gershenzon, Prof. Dr. T. E. Skinner
Physics Department, Wright State University
Dayton, OH 45735 (USA)
E-mail: thomas.skinner@wright.edu
[+] These authors contributed equally to this work.

[**] F.S. thanks Fonds der Chemischen Industrie for financial support. L.W. acknowledges a Longterm EMBO postdoctoral fellowship (grant number ALTF 1520-2011). This research has been supported by the DFG (grant numbers GI 203/7-1 to S.J.G and SFB1035 to M.S.), Fonds der Chemischen Industrie (to S.J.G.), the National Science Foundation (grant number CHE-1214006 to T.E.S), and an allocation of computing time from the Ohio Supercomputing Center (T.E.S.)

Supporting information for this article is available on the WWW under http://dx.doi.org/10.1002/anie.201400178.

diagonal peak can affect spectral analysis. The tolerable limits on sideband intensity as a fraction of the diagonal peak are thus very stringent.

^{13}C-edited NOESY spectra are typically collected using the GARP-4 composite pulse[3b,c] or WURST[3f,g] decoupling schemes. GARP-4 is known for low-intensity sideband artifacts.[3b,c] Unfortunately, the bandwidth of GARP-4 decoupling for a maximum average power of $\gamma B_{1,RMS}/(2\pi) = 4.5$ kHz (a typical limit on cryoprobes) is 25 kHz, which is only adequate at 600 MHz, as illustrated in Figure 1. Thus, at higher fields, two experiments are typically collected with the carrier frequency set to the center of the aliphatic region (ca. 40 ppm) and the center of the aromatic region (ca. 130 ppm), effectively doubling the experiment time. WURST decoupling, based on adiabatic inversion pulses, provides broadband decoupling at low radiofrequency (RF) field strengths, but with sideband artifacts that can be substantial. A conventional alternative is the STUD + decoupling scheme,[4c] which employs an adiabatic hyperbolic secant (sech/tanh) pulse and is able to achieve sideband performance comparable to GARP-4.[6]

An additional consideration is the increased spectral resolution afforded by high-field magnets, which requires longer evolution times for indirectly detected spins, such as the carbon dimension of the ^{13}C-edited NOESY[7] or HCCH-TOCSY.[8] Non-uniform sampling (NUS) can be employed to collect spectra with optimal resolution in a reasonable experimental time.[7–9] However, the time domain data collected with NUS must be reconstructed before Fourier transform, which can lead to spectral artifacts.[10] NUS sampling artifacts arise from all signals in a spectrum, whether they originate from the sample or from an experimental artifact such as a decoupling sideband.[10]

Thus, especially for applications at high magnetic fields (i.e. 900 MHz ^{1}H frequency and above) there is a great need for a robust, low-power, broadband ^{13}C decoupling pulse with the lowest possible sideband artifacts. Here, we introduce a low power pulse capable of decoupling ^{13}C spins with minimal sideband artifacts in a single scan. The pulse is named BUSS for broadband uniform sideband suppression and represents a new generation of decoupling pulses free from the constraints of periodic and cyclic sequences imposed on the solution space.

The evolution of a spin system during an NMR experiment is described by the Liouville-von-Neumann equation of motion and can be actively steered through the irradiation of radiofrequency (RF) pulses. The optimization of pulse sequences under certain quality criteria based on methods of optimal control theory can be achieved through algorithms that numerically optimize the external controls, namely the RF pulses. This approach has been successfully applied to various problems and was first demonstrated for frequency-selective pulses.[11] The GRAPE algorithm (gradient ascent pulse engineering) allows the optimization of NMR pulse sequences efficiently in very large parameter spaces.[12] It has been successfully used for the design of broadband and robust excitation, inversion, and refocusing pulses in uncoupled spin systems[12,13] exemplifying the power and versatility of optimal control theory in finding non-intuitive solutions for complex spin dynamics. Although global optimality is not guaranteed for such a numerical optimization approach, it has been demonstrated, for example, in heteronuclear coherence transfer experiments, that the numerically optimized pulses achieved the analytically derived maximal transfer efficiency in terms of time-optimal and relaxation-optimal pulses.[14]

A generalized version of the GRAPE algorithm has been developed and applied to the design of single-scan low-power heteronuclear decoupling sequences for in vivo applications.[15] Here, we apply this concept to the optimization of novel single-scan ultra-broadband decoupling sequences producing minimal sideband amplitudes at power levels achievable by standard probes. Instead of optimizing the evolution of the spin system from an initial state to a target final state, this approach tracks and optimizes the evolution of the magnetization over a number of acquisition points throughout the whole decoupling pulse sequence. This optimal tracking approach is especially suited for optimizing heteronuclear decoupling sequences with the goal of inhibiting or scaling the coupling evolution throughout the free induction decay (FID) by irradiating one spin while observing the other.[15,16] In contrast to conventional approaches based on average Hamiltonian theory, which result in periodic patterns of inversion pulses, optimal tracking can steer the coupled spin system to a desired trajectory as closely as possible without imposing periodicity on the RF control amplitudes. In addition, constraints on the optimization representing experimental limitations, such as power limits, or robustness with regard to B_1 inhomogeneities, can be taken into account.[17]

To create a broadband pulse for use at ultra-high magnetic fields, a target decoupling bandwidth of 45 kHz, which will cover the entire ^{13}C chemical shift range at 28.2 T (corresponding to 1.2 GHz proton Larmor frequency) for proteins and nucleic acids was used as a constraint. The maximum power recommendation for heteronuclear decoupling on modern cryoprobes was considered as an additional constraint during optimization. Typical power limitations for modern cryoprobes are $\gamma B_{1,RMS}/(2\pi) = 4.5$ kHz for a total duration of about 140 ms (e.g. manufacturers suggested threshold for cryoprobes). Therefore, this limitation was used as a target maximum average power for optimal tracking constraints and for comparison with the composite and adiabatic decoupling sequences. Ideal decoupling of a zero-frequency center peak is attained if the J-coupling evolution is refocused at each acquisition point. Deviations from this ideal represent modulations of the signal that appear as the aforementioned sidebands.

A simple variation in the optimal tracking algorithm employed here was to apply the tracking at each time-step of the RF waveform, which is most typically much faster than the sampling rate. The algorithm cannot achieve complete J-refocusing during all times of the sequence, but asking it to do so forces it to search for the closest approach to this ideal and results in a decoupling sequence that is not constrained to a particular sampling rate. The waveform was digitized in increments of 4.3 μs and the pulse was optimized over the entire offset range (−23.5 to 23.5 kHz, 117.5 Hz increments, 401 offset points) using a coupling strength $J = 150$ Hz.

Further details of the optimization procedure as applied to decoupling can be found in Ref. [15] and the supplement.

The converged calculation resulted in the BUSS pulse that meets the target constraints by decoupling a 45 kHz bandwidth and producing exceptionally low sideband intensities using only 4.4 kHz $\gamma B_{1,RMS}/(2\pi)$. The performance of the BUSS pulse was compared in simulations and experiments to GARP-4 composite pulse decoupling,[3b,c] adiabatic STUD + decoupling[4c,d] (sech/tanh), and the caWURST-2 decoupling scheme,[3g] a constant adiabaticity[3g,18] variant of the WURST pulses[3f] widely used for broadband decoupling. Parameters for caWURST-2 were calculated using the Bruker shape tool to generate the standard implementation that is available to the general user. Details for each pulse scheme are listed in Table S1.

Decoupling performance was verified using the isolated ^{1}H-^{13}C two-spin system ($J = 197$ Hz) in ^{13}C-labeled sodium formate, where the observed proton doublet collapses into a single peak when the ^{1}H-^{13}C coupling is effectively removed. The decoupled bandwidth for each decoupling scheme is shown in Figure S1. BUSS decouples the center peak across the entire 45 kHz bandwidth by more than 98%, as seen in the simulations. At the same $\gamma B_{1,RMS}/(2\pi)$, the BUSS and adiabatic pulses clearly outperform composite pulse decoupling in terms of bandwidth. Although the BUSS pulse was optimized for $J = 150$ Hz, it provides excellent performance for a broad range of heteronuclear J-coupling constants as high as about 200 Hz. As expected, sideband intensities decrease for smaller J-couplings as can be seen in simulations for $J = [90, 130, 197]$ Hz (Figure S2).

The advantage of using GARP-4 composite pulse decoupling is its low sideband production at distinct frequency offsets in the observed spectrum (in this case ^{1}H), which makes it especially valuable for application with NOESY experiments. Figure 2 shows, for all four decoupling schemes, contour plots of simulated and experimental sideband intensities over a ^{1}H offset range ± 1000 Hz relative to the center peak and over a ^{13}C decoupler offset range $\pm 30\,000$ Hz relative to the decoupled ^{13}C resonance frequency.

Within the decoupled offset range, the BUSS pulse clearly has the lowest sideband artifacts. At the same average decoupling strength, the caWURST-2 pulse has sideband intensities at a level of up to 3.0% of the decoupled peak at harmonics of 1/pulse duration. The sech/tanh pulse achieves sideband levels comparable to GARP-4 and, in addition, decouples the entire required bandwidth.

However, as shown in Figure S3, sech/tanh has a multitude of additional sidebands compared to GARP-4, which can lead to unwanted baseline distortions in decoupled spectra. The significantly improved quality of BUSS decoupling is compared to the other decoupling schemes in Figure 3, where the root-mean-square of the sideband amplitudes summed over the decoupled ^{13}C offsets ($\pm 12\,500$ Hz for GARP-4 and $\pm 22\,500$ Hz for the rest) are plotted as a function of offset from the ^{1}H center peak frequency. Figure S3 compares the experimental and simulated sidebands in an overlay of all sidebands in the decoupled ^{13}C offset range for each decoupling scheme, highlighting the maximum sideband intensities. The sideband artifacts are for all schemes slightly

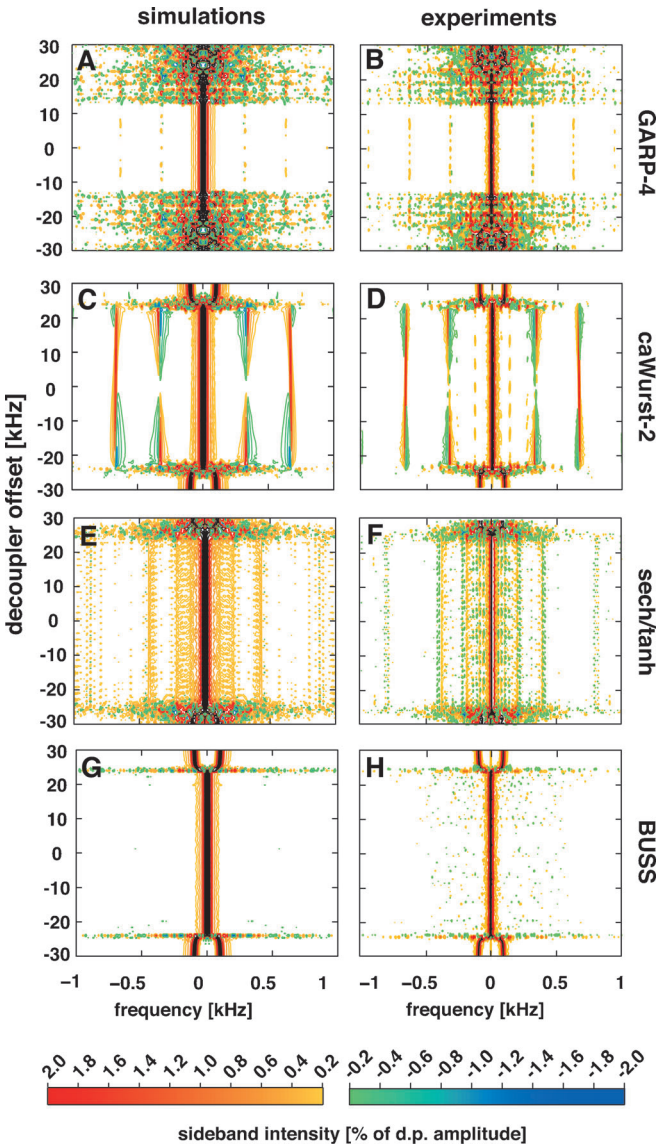

Figure 2. Contour plots comparing the simulated (left panels) and experimental (right panels) sideband distribution across a decoupler offset range of 60 kHz discretized in 101 steps for GARP-4 (A, B), caWURST-2 (C, D), sech/tanh (E, F), and BUSS (G, H) decoupling pulses. Contour lines in black are given from 100% to 5% of the decoupled peak amplitude. Contour lines in color are plotted at (2, 1.5, 1, 0.5, 0.3, and 0.2%) and (−2, −1.5, −1, −0.5, −0.3, and −0.2%) of the decoupled peak (d.p.) amplitude to highlight the decoupling sidebands. Axes labels apply to all graphs.

higher in experiments as compared to simulations (Figure 2 and Figure S3). This effect is likely due to non-ideal B_1 calibration in the experiment. Simulations show that the BUSS pulse has similar robustness with regard to B_1 inhomogeneity as conventional decoupling pulses (see Figures S4 and S5). Within the limits of most modern probes (± 10%) the BUSS pulse performs exceptionally well.

The performance of the BUSS pulse was compared to GARP-4, sech/tanh, and caWURST-2 decoupling schemes in ^{13}C-decoupled ^{1}H,^{1}H NOESY experiments. Figure 4 A shows an overlay of NOESY spectra collected with BUSS pulse

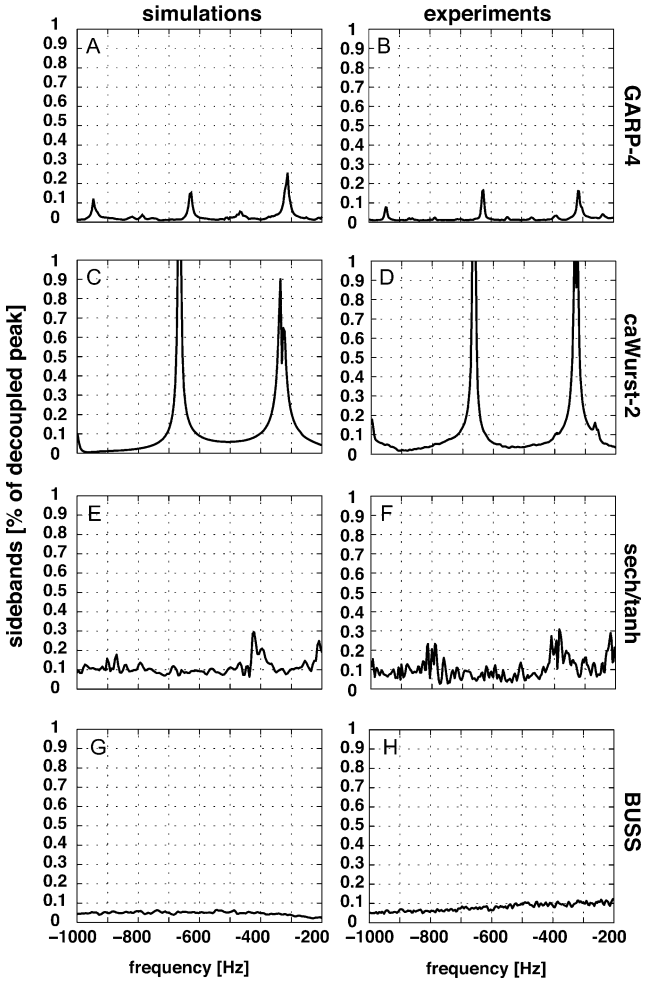

Figure 3. Simulated (left panels) and experimental (right panels) root-mean-square sideband amplitudes across the decoupled offset range for A,B) GARP-4 (24 kHz), C,D) caWURST-2 (45 kHz), E,F) sech/tanh (45 kHz), and G,H) BUSS (45 kHz). Since the sideband spectra are symmetric with respect to the decoupled ^{1}H center peak of Figure 2 only the spectral region from −200 Hz to −1000 Hz on the left hand side of Figure 2 is depicted. Axes labels apply to all graphs.

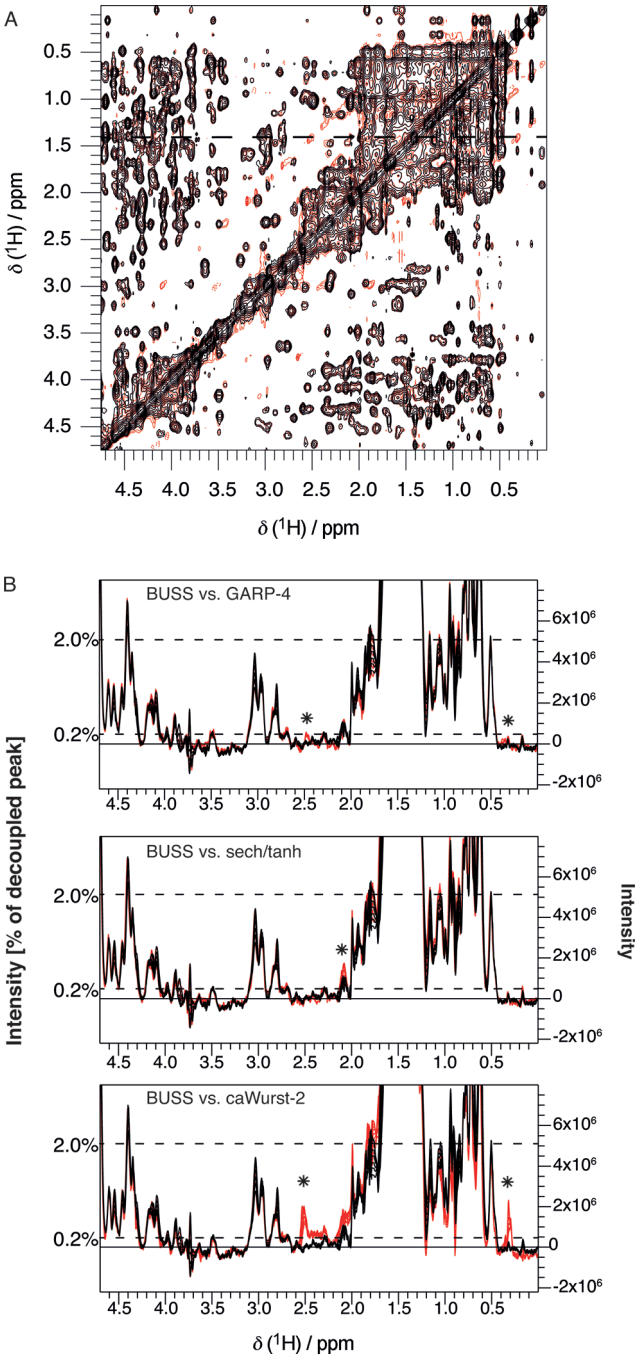

Figure 4. ^{1}H,^{1}H NOESY spectra collected with ^{13}C decoupling. A) Overlay of the 2D spectra collected with BUSS (black) and caWURST-2 (red) decoupling. Contours are set to 1% of the decoupled peak intensity at 1.4 ppm. B) Overlay of 1D traces through 1.40±0.05 ppm from the spectrum collected with BUSS (black) and GARP-4, sech/tanh, and caWURST-2 (all in red). Asterisks mark the decoupling sidebands. Axes labels apply to all graphs.

decoupling (black) and caWURST-2 (red). Significant off-diagonal artifact peaks are produced by caWURST-2, which makes accurate spectral interpretation difficult. Figure 4B and Figures S6–7 show overlays of 1D traces at several ^{1}H offsets comparing BUSS decoupling to the other decoupling schemes. The sideband artifacts are marked with an asterisk. The sidebands from GARP-4 and sech/tanh decoupling are small and generally below the 0.2% threshold. However, the intensity of a peak, the frequency of which is the same as the sideband frequency, will be inaccurately interpreted. Quantitative experiments that rely on accurate measures of peak intensities such as NOESY experiments will clearly benefit from using BUSS over GARP-4 or sech/tanh. As seen in the simulations and experimental examples with ^{13}C sodium formate (Figure 2, Figure 3), the caWURST-2 pulse has intense sideband intensities at harmonics of 1/pulse duration, rendering it impractical for use in NOESY. Although the intensity and location of sideband artifacts from adiabatic decoupling could be minimized by using higher power, this will induce sample heating, can exceed probe limitations and is antithetical to the objective here of low-power broadband decoupling.

In conclusion, we presented a novel noncyclic, single-scan decoupling pulse (BUSS) and demonstrated that it provides

substantially improved performance compared to existing state-of-the-art decoupling schemes. BUSS decoupling is thus a preferable alternative for ultra-broadband decoupling with minimal sideband amplitudes at low power. Compared to conventional decoupling schemes based on average Hamiltonian theory, this next generation of decoupling pulses exploits the flexibility and power of optimal control theory. For biomolecular NMR applications, the BUSS pulse exceeds the performance of conventional composite pulse and adiabatic decoupling and fulfills all of the requirements for heteronuclear decoupling at 1.2 GHz. Further, this approach will also be useful for decoupling other nuclei with very large chemical shift ranges (e.g. ^{19}F) in biomolecular and small-molecule NMR applications. BUSS performs at least as well as adiabatic decoupling pulses with regard to robustness to B_1 inhomogeneity. This performance can be improved by employing additional constraints in the optimal control algorithm for applications that exhibit more significant non-homogenous B_1 distributions, such as in low-field NMR or in vivo spectroscopy.[19] We note that further robustness and reduction of sidebands can be achieved through application of multi-scan cooperative pulses[20] to heteronuclear decoupling. Developing such methods is on-going but beyond the scope of the current study, which focuses on decoupling in a single scan.

Received: January 7, 2014
Published online: March 12, 2014

Keywords: NMR spectroscopy · nucleic acids · proteins · decoupling sidebands · ultra-broadband decoupling

[1] W. A. Anderson, R. Freeman, *J. Chem. Phys.* **1962**, *37*, 85 – 103.
[2] R. R. Ernst, *J. Chem. Phys.* **1966**, *45*, 3845 – 3861.
[3] a) M. H. Levitt, R. Freeman, T. Frenkiel, *Adv. Magn. Reson.* **1983**, *11*, 47 – 110; b) A. J. Shaka, P. B. Barker, R. Freeman, *J. Magn. Reson.* **1985**, *64*, 547 – 552; c) A. J. Shaka, J. Keeler, *Prog. Nucl. Magn. Reson. Spectrosc.* **1987**, *19*, 47 – 129; d) Z. Starcuk, K. Bartusek, Z. Starcuk, *J. Magn. Reson. Ser. A* **1994**, *107*, 24 – 31; e) M. R. Bendall, *J. Magn. Reson. Ser. A* **1995**, *112*, 126 – 129; f) E. Kupce, R. Freeman, *J. Magn. Reson. Ser. A* **1995**, *115*, 273 – 276; g) E. Kupce, R. Freeman, *J. Magn. Reson. Ser. A* **1996**, *118*, 299 – 303.
[4] a) M. H. Levitt, R. Freeman, T. Frenkiel, *J. Magn. Reson.* **1982**, *50*, 157 – 160; b) T. Fujiwara, K. Nagayama, *J. Magn. Reson.* **1988**, *77*, 53 – 63; c) M. R. Bendall, T. E. Skinner, *J. Magn. Reson.* **1998**, *134*, 331 – 349; d) T. E. Skinner, M. R. Bendall, *J. Magn. Reson.* **1997**, *124*, 474 – 478.
[5] H. Arthanari, G. Wagner, N. Khaneja, *J. Magn. Reson.* **2011**, *209*, 8 – 18.
[6] a) M. S. Silver, R. I. Joseph, D. I. Hoult, *J. Magn. Reson.* **1984**, *59*, 347 – 351; b) F. T. Hioe, *Phys. Rev. A* **1984**, *30*, 2100 – 2103.
[7] V. Tugarinov, L. E. Kay, I. Ibraghimov, V. Y. Orekhov, *J. Am. Chem. Soc.* **2005**, *127*, 2767 – 2775.
[8] B. E. Coggins, P. Zhou, *J. Biomol. NMR* **2008**, *42*, 225 – 239.
[9] a) D. Rovnyak, D. P. Frueh, M. Sastry, Z. Y. Sun, A. S. Stern, J. C. Hoch, G. Wagner, *J. Magn. Reson.* **2004**, *170*, 15 – 21; b) D. Rovnyak, J. C. Hoch, A. S. Stern, G. Wagner, *J. Biomol. NMR* **2004**, *30*, 1 – 10.
[10] M. Mobli, J. C. Hoch, *Concepts Magn. Reson. Part A* **2008**, *32*, 436 – 448.
[11] S. Conolly, D. Nishimura, A. Macovski, *IEEE Trans. Med. Imag.* **1986**, *5*, 106 – 115.
[12] N. Khaneja, T. Reiss, C. Kehlet, T. Schulte-Herbruggen, S. J. Glaser, *J. Magn. Reson.* **2005**, *172*, 296 – 305.
[13] a) B. Luy, K. Kobzar, T. E. Skinner, N. Khaneja, S. J. Glaser, *J. Magn. Reson.* **2005**, *176*, 179 – 186; b) T. E. Skinner, K. Kobzar, B. Luy, M. R. Bendall, W. Bermel, N. Khaneja, S. J. Glaser, *J. Magn. Reson.* **2006**, *179*, 241 – 249; c) N. I. Gershenzon, K. Kobzar, B. Luy, S. J. Glaser, T. E. Skinner, *J. Magn. Reson.* **2007**, *188*, 330 – 336; d) M. A. Janich, R. F. Schulte, M. Schwaiger, S. J. Glaser, *J. Magn. Reson.* **2011**, *213*, 126 – 135; e) K. Kobzar, S. Ehni, T. E. Skinner, S. J. Glaser, B. Luy, *J. Magn. Reson.* **2012**, *225*, 142 – 160.
[14] N. Khaneja, B. Luy, S. J. Glaser, *Proc. Natl. Acad. Sci. USA* **2003**, *100*, 13162 – 13166.
[15] J. L. Neves, B. Heitmann, N. Khaneja, S. J. Glaser, *J. Magn. Reson.* **2009**, *201*, 7 – 17.
[16] a) F. Schilling, S. J. Glaser, *J. Magn. Reson.* **2012**, *223*, 207 – 218; b) G. N. Zhang, F. Schilling, S. J. Glaser, C. Hilty, *Anal. Chem.* **2013**, *85*, 2875 – 2881.
[17] T. E. Skinner, N. I. Gershenzon, S. J. Glaser in *52nd Experimental Nuclear Magnetic Resonance Conference*, Asilomar, **2011,** *Abstract 114*.
[18] A. Tannús, M. Garwood, *J. Magn. Reson. Ser. A* **1996**, *120*, 133 – 137.
[19] R. A. de Graaf, *Magn. Reson. Med.* **2005**, *53*, 1297 – 1306.
[20] M. Braun, S. J. Glaser, *J. Magn. Reson.* **2010**, *207*, 114 – 123.

